



CHORUS

This is the accepted manuscript made available via CHORUS. The article has been published as:

Magnon and electromagnon excitations in multiferroic DyFeO_3

T. N. Stanislavchuk, Yazhong Wang, Y. Janssen, G. L. Carr, S.-W. Cheong, and A. A. Sirenko
Phys. Rev. B **93**, 094403 — Published 4 March 2016

DOI: [10.1103/PhysRevB.93.094403](https://doi.org/10.1103/PhysRevB.93.094403)

Magnon and electromagnon excitations in multiferroic DyFeO₃

T. N. Stanislavchuk^{1,*}, Yazhong Wang,² Y. Janssen,³ G. L. Carr,⁴ S.-W. Cheong,² and A. A. Sirenko¹

¹ *Department of Physics, New Jersey Institute of Technology, Newark, New Jersey 07102, USA*

² *Rutgers Center for Emergent Materials and Department of Physics and Astronomy, Rutgers University, Piscataway, New Jersey 08854, USA*

³ *Department of Chemistry, Stony Brook University, Stony Brook, NY 11794, USA*

⁴ *National Synchrotron Light Source, Brookhaven National Laboratory, Upton, NY 11973, USA*

Abstract

Optical properties of orthorhombic DyFeO₃ single crystals have been studied in the far-infrared spectral range 11 – 120 cm⁻¹ at the temperatures between 1.5 K and 50 K and magnetic fields H up to 7 T. The temperature and magnetic-field dependencies of the antiferromagnetic (AFM) resonance spectra have been measured below and above the AFM ordering temperature of Dy³⁺ moments with $T_N^{\text{Dy}} = 4.2$ K. Hardening of the quasi-ferromagnetic mode frequency of the AFM resonance due to ordering of Dy³⁺ moments is observed. Below T_N^{Dy} two electric dipole-active

* Author to whom correspondence should be addressed. Electronic mail: stantar@njit.edu

magnetic excitations, or electromagnons, appear in the spectra at 20 cm^{-1} and 60 cm^{-1} . The electromagnons vanish with the application of a strong magnetic field along the a or b axis which changes the magnetic structures of Fe^{3+} and Dy^{3+} moments into the ones compatible with the spatial inversion symmetry. We show that the electromagnon at $\sim 20 \text{ cm}^{-1}$ provides a significant contribution to the static electric permittivity ϵ . The energies of the electromagnons as well as static electric permittivity manifest a strong hysteresis upon cycling of external magnetic field at $T < T_N^{\text{Dy}}$.

PACS: 75.85.+t, 75.30.Ds, 78.20.Ls, 78.30.-j

I. INTRODUCTION

Rare earth orthoferrites crystalize in the orthorhombically distorted perovskite structure ($Pbnm$) with four $RFeO_3$ molecules per unit cell [1]. In all studied orthoferrites the Fe–Fe exchange interaction leads to an antiferromagnetic (AFM) ordering of the Fe subsystem with a weak ferromagnetic (FM) canting due to Dzyaloshinsky-Moriya interaction at Neel temperatures T_N in the range between 650 K and 700 K [2]. The resulted spin structure $\Gamma_4 (G_x A_y F_z)$ persists down to the lowest temperatures in orthoferrites with non-magnetic R -ions ($R=Y, La, \text{ and } Lu$). In other $RFeO_3$ compounds, the magnetic rare-earth ions are polarized by R –Fe exchange interaction and the degree of polarization increases with the temperature decrease. The increase of polarization results in increase of magnetic anisotropy of rare-earth subsystem that can lead to a spin-reorientation (SR) transition. In most rare-earth orthoferrites, the SR transition occurs via two second-order phase transitions, which result in the change of the spin configuration of Fe subsystem from $\Gamma_4 (G_x A_y F_z)$ with the net magnetization directed along the c -axis to $\Gamma_2 (F_x C_y G_z)$ with the net magnetization directed along the a -axis. $DyFeO_3$ is the only non-substituted member of the orthoferrite family in which the spin configuration of Fe subsystem changes from weakly ferromagnetic Γ_4 to purely AFM $\Gamma_1 (A_x G_y C_z)$ via the Morin-type phase transition at $T_M = 50$ K [3, 4]. In the temperature range between 1.5 K and 4 K several orthoferrites show spin ordering of the rare-earth subsystem. In particular, Dy^{3+} spins order antiferromagnetically in $\Gamma_5 (g_x a_y)$ spin configuration at $T_N^{Dy} \approx 4$ K [3, 5]. Application of high enough magnetic field along the principal crystallographic axes of $DyFeO_3$ results in SR phase transitions [4, 6]. For example, application of magnetic field along the a -axis results in spin screw transition of Fe subsystem from Γ_1 configuration to Γ_2 one, application along the b -axis – in spin-flop transition from Γ_1 to Γ_4

configuration, and application along the c -axis – in spin-screw transition from Γ_1 to Γ_4 configuration.

Spin configurations Γ_1 , Γ_2 and Γ_4 observed in the Fe subsystem of DyFeO_3 (and other rare-earth orthoferrites) are compatible with the space inversion operation and, hence, do not allow neither linear magnetoelectric effect nor spontaneous electric polarization. Below T_N^{Dy} , Dy moments order into Γ_5 ($g_x a_y$) configuration which together with Γ_1 configuration of Fe spins form a 222 non-polar magnetic symmetry group. This symmetry still doesn't allow spontaneous ferroelectric polarization but, due to breaking of inversion symmetry, allows linear magnetoelectric effect with diagonal components of the magnetoelectric tensor α_{ii} ($i = x, y, z$) [7]. A magnetic field applied along the c axes can reorient Fe spins from Γ_1 to Γ_4 configuration that together with Γ_5 Dy spin configuration results in a polar magnetic group $2m'm'$ and, hence, existence of spontaneous polarization along the c -axis becomes possible (the ME tensor remains diagonal so that $\alpha_{zz} \neq 0$). The appearance of spontaneous polarization along the c -axis in DyFeO_3 below T_N^{Dy} and in high magnetic fields $H||c$ (Fe spins are in the Γ_4 configuration) was reported by Tokunaga *et al.* [8]. The exchange striction between adjacent Fe^{3+} and Dy^{3+} layers was proposed as the origin of the ferroelectric polarization in the low-temperature multiferroic phase [8].

Ordering of Dy moments below T_N^{Dy} allows for a linear magnetoelectric effect and, hence, opens up a possibility for observation of dynamic magnetoelectric effects in a form of so-called electromagnons - magnetic resonances excited by electric E vector of light [9, 10, 11]. Literature on electromagnons in magnetic oxides includes perovskite RMnO_3 [12,13,14,15,16], hexagonal YMnO_3 [17], RMn_2O_5 [18], $\text{Ba}_2\text{CoGe}_2\text{O}_7$ [19] and CuO [20] compounds. In iron-based multiferroics

electromagnons were reported in BiFeO_3 [^{21,22}], $\text{SmFe}_3(\text{BO}_3)_4$ [²³], $\text{Ba}_2\text{Mg}_2\text{Fe}_{12}\text{O}_{22}$ [^{24,25}] and $\text{CuFe}_{1-x}\text{Ga}_x\text{O}_2$ [²⁶]. Although electromagnons were observed in a number of magnetoelectric materials, electromagnon spectra were not reported so far for rare-earth orthoferrites.

The spinwave spectrum of Fe subsystem in DyFeO_3 consists of four modes of homogeneous magnetic oscillations, two of which are exchange modes with frequencies $\sim 1000 \text{ cm}^{-1}$ and the other two are acoustic modes, which at $k=0$ correspond to quasi-ferromagnetic (quasi-FM) and quasi-antiferromagnetic (quasi-AFM) resonances with frequencies below 20 cm^{-1} . The properties of the last two excitations were studied in literature only above the temperature of Dy-spin ordering using Raman scattering [^{27, 28}], infrared (IR) spectroscopy [²⁹], and neutron scattering [³⁰]. At room temperature the frequency of the quasi-AFM mode is $\sim 17 \text{ cm}^{-1}$ and is higher than the frequency of the quasi-FM mode that is $\sim 13 \text{ cm}^{-1}$. With decreasing temperature, the sharp softening of the quasi-AFM mode occurs: it crosses the quasi-FM mode, and reaches its minimum at the point of Morin-type SR transition at $T_M=50 \text{ K}$. At the same time, the frequency of quasi-FM mode doesn't show any peculiarities at the SR phase transition. With further decrease of the temperature, the frequency of the quasi-AFM mode increases and reaches $\sim 8 \text{ cm}^{-1}$ at $T=4.2 \text{ K}$. The strongest anomalies at the SR phase-transition were observed for the values of magnon oscillator strengths and damping constants which exhibit pronounced discontinuities [²⁹].

While the properties of magnetic excitations were carefully studied in literature at $T>4.2 \text{ K}$, there are no experimental data on magnons' behavior for combination of the low temperatures ($T<4.2 \text{ K}$) and strong magnetic fields, when the magnetic ordering of Dy subsystem occurs. The purpose of this paper is to study magnetic excitations in the vicinity of phase transitions at temperatures down to 1.5 K and in the external magnetic fields up to 7 T . We also report on the observation of

two electromagnons positioned at ~ 20 and ~ 60 cm^{-1} which appear in the spectra below the temperature of Dy magnetic ordering, *i.e.* in magnetoelectric phase of DyFeO_3 .

II. EXPERIMENT

The floating zone growth technique was utilized to produce bulk crystals of DyFeO_3 . Single crystals were oriented using X-ray diffraction, cut and mechanically polished in a form of platelets oriented along the orthorhombic a , b , and c directions. The in-plane cross section areas were about 5×5 mm^2 and the 0.3 mm thickness of all samples was optimized for transmission measurements. To minimize the interference fringes in optical experiments, the opposite sides of the samples were wedged at an angle of about 5 deg. The transmission experiments were carried out at the National Synchrotron Light Source (NSLS), Brookhaven National Laboratory, at the U4IR beamline equipped with a Bruker i66v IR spectrometer and a LHe-pumped (~ 1.6 K) bolometer. Far-IR transmittance spectra were measured using synchrotron radiation with a spectral resolution of 0.3 cm^{-1} in the spectral range between 11 and 230 cm^{-1} . The low-frequency cutoff was determined by diffraction at the entrance diamond window for U4IR beamline. The light polarization in transmission experiments was controlled by wire-grid linear polarizers. An external magnetic field of up to 7 T was applied in the Faraday configuration, so that the directions of the light propagation and the field coincided. Correspondingly, the electric and magnetic fields of light were always perpendicular to external magnetic field. In the text below we will use the notation of transmission geometry where a sub-index of the electric or magnetic fields of light will indicate its direction with respect to crystallographic axes. For example, $e_a h_b$ configuration means that electric field of light \vec{e} is along the a -axis, magnetic field of light \vec{h} is along the b -axis, and the direction of light propagation and external magnetic

field (if any) are both along the missing third index: the c -axis. The raw data of transmittance spectra were normalized to transmission through an empty aperture with a size equal to that of the sample. For samples with strong thickness interference fringes we normalized the transmitted intensity to that measured at high temperature or high magnetic fields, where no magnons were present. Temperature and magnetic field dependencies for static values of $\epsilon(H,T)$ were measured using an LCR meter at 27 kHz.

III. EXPERIMENTAL RESULTS

3.1 Far-IR spectra of magnons and electromagnons in a zero magnetic field.

In this Section we will discuss temperature and magnetic field dependencies of transmittance spectra of DyFeO₃ in the far-infrared spectral range in several complementary experimental configurations $e_b h_a$, $e_c h_a$, $e_b h_c$, and $e_c h_b$. The magnon temperature dependencies and corresponding transmittance maps for the frequency-temperature parameter space are shown in Figs. 1, 2, 3, and 4 for $e_b h_a$, $e_c h_a$, $e_b h_c$, and $e_c h_b$ configurations, respectively. To interpret the spectra of magnons we used the selection rules for magnetic dipole excitation of quasi-FM and quasi-AFM modes of AFMR in $Pbnm$ structure of DyFeO₃ [³¹, ³²], which are summarized in Table I. In this section we will focus first on the temperature behavior of the magnon and electromagnon modes at $H=0$. After that we will describe the magnetic field dependencies of the magnons and electromagnons.

Quasi-FM mode.

Figure 1 shows temperature dependence of transmission spectra in the $e_b h_a$ configuration below Morin-type phase transition temperature $T_M \sim 50$ K when iron spins are in $\Gamma_1(G_y)$ configuration. The experimental spectra are dominated by one absorption line positioned between 12 and 14 cm^{-1} at $T > 4.2$ K. This line is observed only in configurations with $h \parallel a$, as one can also see in the complementary $e_c h_a$ configuration (Fig. 2). We attribute it to the quasi-FM mode which, according to Table 1, can be excited by h_a component of electromagnetic field only in $\Gamma_1(G_y)$ phase. This interpretation is in agreement with Balbashov *et al.* [²⁹] where a quasi-FM mode of AFMR positioned at 14 cm^{-1} was observed in transmission spectra of DyFeO_3 with $h \perp c$ at $T \geq 4$ K. The main new experimental finding is that at $T < 4.2$ K the frequency of the quasi-FM mode increases from 14 cm^{-1} to 19 cm^{-1} . This magnon hardening at low temperatures can be naturally attributed to the magnetic ordering of Dy spins in the ab plane.

Quasi-AFM mode.

Figure 3 shows temperature dependence of transmission spectra in the $e_b h_c$ configuration for the temperature range between 1.5 K and 10 K. Below $T_N^{\text{Dy}} = 4.2$ K, a narrow absorption line is observed at ~ 14 cm^{-1} . This line is observed only in $h \parallel c$ configurations at $T < T_N^{\text{Dy}}$. For example it is also observed in the magnetic field dependence of transmission spectra in the $e_a h_c$ configuration at $H = 0$ T and $T = 1.5$ K (see Fig. 5). Thus we attribute this line to a purely magnetic dipole polarized along the c -axis. We note here that this magnon mode is clearly distinguished from the quasi-FM one as the latter has energy of about 19 cm^{-1} at $T = 1.5$ K (see Fig. 1). We assume that the excitation we observe in Figs. 3 and 5 is a quasi-AFM mode. Indeed, in $\Gamma_1(G_y)$

phase of Fe spins quasi-AFM mode can be excited by h_c component of electromagnetic field only (see Table I). Balbashov *et al.* [29] reported the observation of quasi-AFM mode in $h||c$ polarized transmission spectra of DyFeO₃. At $T=4.2$ K the quasi-AFM mode's energy is 8 cm^{-1} that is beyond our accessible spectral range, and thus we cannot observe it in our spectra. But as temperature goes below $T_N^{Dy}=4.2$ K, the AFM ordering of Dy spins enhances the energy of the quasi-AFM mode from 8 cm^{-1} at $T=4.2$ K to 14 cm^{-1} at $T=1.5$ K that is now falling into the accessible spectral range for our measurements. The increase of the quasi-AFM mode energy by 6 cm^{-1} is quite reasonable taking into account that magnetic ordering of Dy spins increases the energy of the quasi-FM mode by 5 cm^{-1} , namely, from 14 cm^{-1} at 4.2 K to 19 cm^{-1} at 1.5 K, as shown in Fig. 1.

Electromagnon excitations.

Figure 2 shows that in the $e_c h_a$ configuration two wide absorption lines appear below T_N^{Dy} : a strong one at $\sim 22 \text{ cm}^{-1}$ denoted as EM₁ and a weaker one at $\sim 60 \text{ cm}^{-1}$ denoted as EM₂. These lines are observed only in the $e||c$ configurations and only below T_N^{Dy} . For example, they are also seen in the $e_c h_b$ configuration at $T < 4.2$ K (see Fig. 4) but cannot be detected in the orthogonal $e_b h_a$ configuration (Fig. 1). Thus, EM₁ and EM₂ lines are electric dipole active along the c -axis. Among the possible candidates for electric dipole excitations in the far-IR spectral region are phonons and crystal-field (CF) transitions in Dy³⁺ ions. The lowest frequency phonon in rare-earth orthoferrites is known to be at $\sim 100 \text{ cm}^{-1}$ [28], which is well above the frequency of the observed two lines. Now let us discuss whether electronic transitions in Dy³⁺ ions can be responsible for EM₁ and EM₂ lines. The Dy ions occupy four sites in the crystalline unit cell of

DyFeO_3 orthoferrite and have two nonequivalent positions described by the point symmetry group C_s . Since Dy^{3+} is a Kramer's ion, *i.e.* has odd number of electrons, the local CF of C_s symmetry splits the multiplets of Dy^{3+} ions into Kramer's doublets, which remain doubly degenerate at the absence of magnetic field (external or internal due to magnetic ordering). Thus, the ground multiplet ${}^6H_{15/2}$ of Dy^{3+} ions is split into 8 doublets by the CF of DyFeO_3 . The early spectroscopic study of DyFeO_3 in the IR spectral region by Schuchert *et al.* in 1960's [33] showed that the first four CF doublets of Dy^{3+} ions are at 0, 52, 147 and 225 cm^{-1} correspondingly. While the Dy^{3+} doublet at 52 cm^{-1} is somewhat close to the observed EM_2 line at $\sim 60 \text{ cm}^{-1}$, EM_1 line at $\sim 22 \text{ cm}^{-1}$ does not correlate with the Dy^{3+} CF spectrum. Furthermore, magnetization [3] and Mössbauer [34] measurements of DyFeO_3 have shown that the ground doublet of Dy^{3+} ions can be interpreted as a close to pure $|\pm 15/2\rangle$ state with the axis of quantization lying in the ab -plane at an angle of $\varphi_0 \approx \pm 60^\circ$ to the a -axis (the signs \pm in the value of φ_0 correspond to two nonequivalent positions of Dy ions). As a result, the g -factor tensor of the ground Dy^{3+} doublet is highly anisotropic: $g_z \approx 19.7$, $g_x = g_y = 0$ (in the $x'y'z'$ coordinate system, z' is directed along the axis of quantization and x' is along the c -axis). Such a big value of g_z should result in splitting of the ground doublet in the external magnetic field applied along (or having projection on) the axis of quantization z' , and thus in shifting of the CF lines corresponding to the transitions from the ground doublet to the excited doublets of the Dy^{3+} ions. As we will show in the next section, the application of the external magnetic field along the a and b crystallographic axes has not lead to any noticeable shift of the EM_1 and EM_2 lines (see Figs. 9 and 11) pointing that they are not related to the CF transitions. Moreover, though the ground doublet of Dy^{3+} does not have a non-zero g -factor along the c -axis, the Dy subsystem does possess an appreciable magnetic susceptibility χ_c along the c -axis at low temperatures [35].

It was shown [36] that χ_c can be explained by Van-Vleck contribution from the first excited CF level of Dy³⁺ ions, and the calculated value of χ_c is in good agreement with the magnetization measurements [35] provided that the first excited CF level is at $\sim 52 \text{ cm}^{-1}$. Finally Mössbauer measurements [34] of DyFeO₃ at temperatures up to 50 K are consistent with population of only the ground Dy doublet, thus proving that the first excited CF level is above 50 K ($\sim 35 \text{ cm}^{-1}$). Based on the above arguments, we can exclude both phonons and electronic transitions from the candidates of excitations responsible for the observed EM₁ and EM₂ absorption lines. We note, that EM₁ and EM₂ lines appear only below T_N^{Dy} , when linear magnetoelectric effect is allowed. As we will show in the next section, the application of strong enough magnetic field along the a or b axis, which changes the magnetic structures of Fe³⁺ and Dy³⁺ moments into the ones compatible with spatial inversion symmetry, results in vanishing of the EM₁ and EM₂ lines (see Figs. 9 and 11). Thus we conclude that these lines are observed only in the magnetoelectric phase of DyFeO₃ and attribute them to electric dipole active magnetic excitations, or electromagnons.

3.2 Far-IR spectra of magnons and CF excitations in external magnetic field

Quasi-FM mode

As it was shown above, in $\Gamma_1(G_y)$ state of Fe spins quasi-FM mode is polarized along the a -axis ($h||a$) and thus is observed in transmission spectra in two complementary configurations: $e_b h_a$ and $e_c h_a$. It is convenient to choose $e_b h_a$ configuration to monitor the behavior of the quasi-FM mode since in this configuration the quasi-FM mode is not overlapped with EM₁ absorption which is observed in the $e_c h_a$ configuration below T_N^{Dy} (see Fig. 2). Figure 6 shows magnetic field

dependence ($H||c$) of the quasi-FM mode measured in the $e_b h_a$ configuration at $T=1.5$ K. At $H=0$ the Fe subsystem is in $\Gamma_1(G_y)$ state and Dy subsystem is in $\Gamma_5(g_x a_y)$ state. With the field increase the magnon's frequency is insensitive to magnetic fields up to $\mu_0 H_{cr}^c \approx 3$ T. At H_{cr}^c the Fe subsystem reorients from $\Gamma_1(G_y)$ state to canted $\Gamma_4(G_x F_z)$ state while the magnetic structure of Dy moments remains unchanged. At $H > H_{cr}^c$ quasi-FM mode frequency ω_{FM} reveals a close to linear dependence on H with the effective g -factor $g_{eff} \approx 2.1$ which we define as follows: $\Delta\omega_{FM} = g_{eff} \mu_B \mu_0 \Delta H$, where $\Delta\omega_{FM}$ is a frequency shift measured in [cm^{-1}] induced by a change of the magnetic field magnitude by ΔH , μ_B is a Bohr magneton ($\mu_B \approx 0.4669 \text{ cm}^{-1}/\text{T}$) and μ_0 is a magnetic constant. The extrapolated value of ω_{FM} at $H > H_{cr}^c$ towards $H=0$ is $\omega_{FM}^{extrap} \approx 15.2 \text{ cm}^{-1}$ which is close to the frequency of quasi-FM mode $\omega_{FM} \Big|_{T=5K}^{H=0} \approx 14 \text{ cm}^{-1}$ in zero field and temperatures just above T_N^{Dy} (see Fig. 1), when Fe spins are in $\Gamma_4(G_x F_z)$ phase and Dy ions are paramagnetic.

Figure 7 shows magnetic field dependence ($H||b$) of transmittance measured in the $e_c h_a$ configuration at $T=5$ K (a,b) and 1.5 K (c,d). At $T=5$ K and $H=0$ the quasi-FM mode is observed at $\sim 14 \text{ cm}^{-1}$. With the field increase above $\mu_0 H_{cr}^b \approx 0.6$ T, the quasi-FM mode vanishes but above 2 T another magnon is observed at $\sim 12.5 \text{ cm}^{-1}$ and its position practically doesn't change with the further increase of magnetic field. The magnetic field applied along the b -axis causes the SR transition of Fe subsystem from $\Gamma_1(G_y)$ to $\Gamma_4(G_x F_z)$ spin configuration [6]. Thus the magnon at $\sim 12.5 \text{ cm}^{-1}$ is observed in $\Gamma_4(G_x F_z)$ phase of Fe spins ($H > H_{cr}^b$) and is magnetic dipole-active along the a -axis ($e_c h_a$ configuration of measurements). Based on selection rules from Table I, we attribute this magnon to the quasi-FM mode, which is active in $\Gamma_4(G_x F_z)$ phase for $h||a$.

At $T=1.5$ K and $H=0$ (Figs. 7(c,d)) the quasi-FM mode, enhanced by Dy ordering, is at ~ 19 cm^{-1} (see, for example, Fig. 1) that falls into the region of EM_1 absorption and is not explicitly observed in our spectra. Above $\mu_0 H_{cr}^b \approx 1.3$ T the EM_1 and quasi-FM mode absorptions vanish due to onset of $\Gamma_1 \rightarrow \Gamma_4$ spin-reorientation transition of Fe spins accompanied by the reorientation of Dy moments from $\Gamma_5 (g_x a_y)$ to $\Gamma_3 (f_y c_x)$ state [37]. At $\mu_0 H_b > 2$ T, the quasi-FM mode appears at ~ 12.5 cm^{-1} (Figs. 7(c,d)) just like in the case of spectra at $T=5$ K (Figs. 7(a,b)). We note, that the frequency of the quasi-FM mode in the field induced Γ_4 state of Fe spins and extrapolated towards $H=0$ is different for $H||c$ ($\omega_{FM}^{extrap} \approx 15.2$ cm^{-1} ; see Fig. 6(b)) and for $H||b$ ($\omega_{FM} \approx 12.5$ cm^{-1} ; see Figs. 7(b,d)). The difference can be due to different magnetic structures of Dy subsystem. For $H||b$ and $T=1.5$ K the Dy structure is $\Gamma_3 (f_y c_x)$ above $\mu_0 H_b \approx 2$ T, where $\omega_{FM} \approx 12.5$ cm^{-1} is observed. For $H||b$ and $T=5$ K the Dy subsystem is paramagnetic and is polarized by the external magnetic field in the $\Gamma_3 (f_y c_x)$ configuration. At $\mu_0 H_b \approx 2$ T the splitting of the ground Dy doublet is $\Delta = g_z \mu_B \mu_0 H_b \sin \varphi_0 \approx 14.5$ cm^{-1} (≈ 20 K). Such a splitting at $T=5$ K means that only the lowest sublevel of the split ground Dy doublet is populated and the magnetization of Dy is close to saturation. Thus magnetic state of Dy moments at $\mu_0 H_b > 2$ T is approximately the same for both $T=5$ K and $T=1.5$ K, which results in the same frequency $\omega_{FM} \approx 12.5$ cm^{-1} of the quasi-FM mode. In contrast to the case of $H||b$, for $H||c$ and $T=1.5$ K the magnetic structure of Dy spins is $\Gamma_5 (g_x a_y)$ and doesn't change with the field increase. The $\Gamma_5 (g_x a_y)$ structure of Dy spins renormalizes the frequency of the quasi-FM mode in a different way than $\Gamma_3 (f_y c_x)$ structure does, which results in the observed difference between $\omega_{FM}^{extrap} \approx 15.2$ cm^{-1} at $H||c$ (see Fig. 6(b)) and $\omega_{FM} \approx 12.5$ cm^{-1} at $H||b$ (see Figs. 7(b,d)).

Quasi-AFM mode

In the $\Gamma_1(G_y)$ state of Fe spins the quasi-AFM mode is polarized along the c -axis ($h||c$) and thus is observed in the $e_a h_c$ and $e_b h_c$ configurations. Figure 8 shows a magnetic field dependence ($H||a$) of transmittance measured in the $e_b h_c$ configuration at $T=1.5$ K. The quasi-AFM mode is observed at $\omega_{AFM} \approx 14 \text{ cm}^{-1}$ for $H=0$ and its frequency is insensitive to magnetic fields up to $\mu_0 H_{cr}^a = 1$ T. Just above H_{cr}^a , another line appears at $\sim 17 \text{ cm}^{-1}$ and its frequency gradually increases and stabilizes at $\sim 23 \text{ cm}^{-1}$ in the field of 2 T. The magnetic field applied along the a -axis causes a spin-screw transition of Fe subsystem from $\Gamma_1(G_y)$ to $\Gamma_2(G_z F_x)$ configurations [^{4,6}] accompanied by spin-reorientation of Dy moments from $\Gamma_5(a_y g_x)$ to $\Gamma_2(f_x c_y)$ state. According to selection rules from Table I, in $\Gamma_2(G_z F_x)$ phase of Fe spins quasi-AFM mode can be excited by h_a component of electromagnetic field only and thus cannot be observed in $e_b h_c$ configuration in Figs. 8(a,b) for $H > H_{cr}^a$. Instead, in $\Gamma_2(G_z F_x)$ phase the conditions for the excitation of quasi-FM mode are $h||b$ or $h||c$. Thus we conclude that the line observed in Figs. 8(a,b) for $H > H_{cr}^a$ is the quasi-FM mode. The fact that its frequency gradually increases and stabilizes at $\sim 23 \text{ cm}^{-1}$ in the field of 2 T might indicate that between 1 T and 2 T Fe spins continue to rotate from Γ_1 structure to Γ_2 structure till they stabilize at 2 T. Indeed, as was shown by Gnatchenko et al. [³⁸] the reorientation of Fe spins in $H||a$ at $T < T_M$ ($T_M=41$ K is a temperature of Morin transition) occurs in a sequence $\Gamma_4(G_y) \rightarrow \Gamma_{12}(F_x G_y G_z) \rightarrow \Gamma_2(F_x G_z)$ through continuous rotation of F and G vectors and is completed by a second order phase transition to a Γ_2 phase. The stabilization of the quasi-FM mode's frequency above 2 T indicates that the

mode's effective g -factor along the a -axis when Fe spins are in Γ_2 phase is negligible in the studied magnetic field region (up to 4 T).

The magnetic field dependence of transmittance ($H||b$) in the $e_a h_c$ configuration at $T=1.5$ K is shown in Fig. 5. The quasi-AFM mode is observed at ~ 14 cm^{-1} at zero magnetic field and its frequency is insensitive to magnetic fields up to $\mu_0 H_{cr}^b \approx 1.3$ T. At $H > H_{cr}^b$ the quasi-AFM mode absorption vanishes. It was shown [4, 6] that magnetic field applied along the b -axis of DyFeO_3 causes spin reorientation of Fe subsystem from Γ_1 (G_y) to Γ_4 ($G_x F_z$) state accompanied by the reorientation of Dy moments from Γ_5 ($a_y g_x$) to Γ_3 ($f_y c_x$) state [37]. In the field induced Γ_4 phase of Fe spins the quasi-AFM mode is excited by h_c component of electromagnetic field, just like in $\Gamma_1(G_y)$ phase (see Table I). Thus the quasi-AFM mode is expected to be observed in $e_a h_c$ spectra for both $H < H_{cr}^b$ (Γ_1 state) and $H > H_{cr}^b$ (Γ_4 state) while in our measurements it was observed only for $H < H_{cr}^b$ (see Fig. 5). As it was shown above, the ordering of Dy subsystem in the Γ_5 ($a_y g_x$) state increases the quasi-FM mode's frequency from 14 to 19 cm^{-1} (see Fig. 1) when the Fe subsystem is in Γ_1 configuration while the field induced ($H||b$) reorientation of Fe spins from Γ_1 (G_y) to Γ_4 ($G_x F_z$) state accompanied by the reorientation of Dy moments from Γ_5 ($a_y g_x$) to Γ_3 ($f_y c_x$) state decreases the quasi-FM mode's frequency from $\omega_{FM} \sim 19$ cm^{-1} (see Fig. 1) down to $\omega_{FM} \sim 12.5$ cm^{-1} (see Figs. 7(b,d)). Previously we concluded that the observation of the quasi-AFM mode at $T=1.5$ K is possible because Dy ordering in the Γ_5 ($a_y g_x$) increases the quasi-AFM mode's frequency from 8 cm^{-1} to 14 cm^{-1} . Hence, we assume that at $H > H_{cr}^b$, when the Fe and Dy subsystems are reoriented into Γ_4 and Γ_3 ($f_y c_x$) configurations

correspondingly, the frequency of the quasi-AFM mode is decreased, just like in the case of ω_{FM} , so that it no longer falls into the spectral region of our measurements.

Electromagnons.

Transmission spectra of DyFeO₃ crystal at zero magnetic field revealed two EM₁ and EM₂ absorption lines at ~ 22 cm⁻¹ and ~ 55 cm⁻¹ which appear at $T < T_N^{Dy}$ and are electric dipole-active along the *c*-axis. Figure 10(b) shows a magnetic field dependence ($H||b$) of transmission spectra in the $e_c h_a$ configuration at $T=1.5$ K in the region from 0 to 2 T. At $H=0$ the EM₁ and EM₂ lines are at ~ 20 cm⁻¹ and ~ 50 cm⁻¹ correspondingly. With the increase of magnetic field, the EM_{1,2} lines become weaker and vanish at $\mu_0 H_{cr}^b \approx 1.3$ T when the spin-reorientations of Fe spins from $\Gamma_1 (G_y)$ to $\Gamma_4 (G_x F_z)$ state and Dy moments from $\Gamma_5 (a_y g_x)$ to $\Gamma_3 (f_y c_x)$ state occur. In contrast to $\Gamma_5 (g_x a_y)$ configuration, the $\Gamma_3 (f_y c_x)$ configuration of Dy moments is compatible with spatial inversion symmetry [7] and thus at $H > H_{cr}^b$, when EM_{1,2} absorptions vanish, the magnetoelectric effect in DyFeO₃ is not allowed. Similar behavior of EM_{1,2} lines is observed in transmission spectra when magnetic field is directed along the *a*-axis. Figure 11(b) shows a magnetic field dependence ($H||a$) of transmission spectra in the $e_c h_b$ configuration at $T=1.5$ K in the region from 0 to 3 T. At $H=0$ the EM₁ and EM₂ lines are at ~ 18 cm⁻¹ and ~ 48 cm⁻¹ correspondingly. At $H_{cr}^a \approx 1$ T the reorientation transition of Fe spins from $\Gamma_1 (G_y)$ to $\Gamma_4 (G_x F_z)$ state and Dy moments from $\Gamma_5 (g_x a_y)$ to $\Gamma_2 (f_x c_y)$ state occur and EM_{1,2} absorptions vanish. Just as in case of $\Gamma_3 (f_y c_x)$ configuration, the $\Gamma_2 (f_x c_y)$ configuration of Dy moments is compatible with spatial inversion and, hence, magnetoelectricity is not allowed [7]. Since EM₁

and EM₂ absorptions are observed only in magnetoelectric phases of DyFeO₃ and, as was shown above, are not related to phonon modes or electronic transitions in Dy³⁺ ions, we attribute them to electric dipole-active magnetic excitations or electromagnons. The existence of electric dipole-active magnetic excitations in rare-earth orthoferrites was theoretically predicted by Yablonskii and Krivoruchko back in 1988 [³⁹] and attributed to rare-earth magnetic modes which are odd under inversion symmetry. Our experimental observation of electromagnons in DyFeO₃ at the temperatures below the magnetic ordering of Dy³⁺ moments is in agreement with that theoretical prediction. The exact mechanisms of such dynamic excitations that definitely include ordered rare-earth spins would require a separate theoretical study. The role of Fe³⁺ spins may not be strong because both EM₁ electromagnon and quasi-FM mode were observed simultaneously in Figs. 2 and 9(c). Note, however, that the appearance of EM₁ correlated with a decrease of the oscillator strength for quasi-FM mode at low temperatures compared to that at $T > 4$ K (see inset in Fig.2) thus indicating a possible contribution of Fe³⁺ spins into formation of electromagnon excitations.

The EM₁ and EM₂ electromagnons demonstrate strong hysteresis upon cycling of external magnetic field along the *b*-axis (see Figs. 9(a-d)). At $H=0$ the EM₁ and EM₂ lines are at ~ 20 cm⁻¹ and ~ 50 cm⁻¹ correspondingly. With the increase of magnetic field along the *b*-axis, the EM_{1,2} lines become weaker and vanish at $\mu_0 H_{cr}^b \approx 1.3$ T. Upon decreasing the magnetic field below H_{cr}^b only one broad electromagnon EM₁ is observed at ~ 30 cm⁻¹. With further decreasing the magnetic field another phase transition takes place at $\mu_0 H_{cr2}^b \sim 0.2$ T and the EM₁ at ~ 30 cm⁻¹ vanishes while the EM₁ at ~ 20 cm⁻¹ appears again, as at zero field. The weak EM₂ electromagnon at 50 cm⁻¹ was not “restored” (at least it is not clearly seen in our spectra) even when we reduced the magnetic field to zero. The observation of EM electromagnon at 30 cm⁻¹

can indicate on the existence of an intermediate state of Fe/Dy magnetic moments upon sweeping the magnetic field down at $T < T_N^{Dy}$ when spin reorientation of Fe subsystem from Γ_4 to Γ_1 configuration takes place. As was shown by Gnatchenko et al. [37] the spin reorientation in DyFeO₃ in $H||b$ and $T < T_N^{Dy}$ can occur in two stages: $\Gamma_1(G_y) \rightarrow \Gamma_{1234}(F_x F_y F_z G_x G_y G_z) \rightarrow \Gamma_4(F_x G_y)$ for Fe spins and $\Gamma_5(g_x a_y) \rightarrow \Gamma_{2358}(g_{xy} a_{xy} f_{xy} c_{xy}) \rightarrow \Gamma_3(f_y c_x)$ for Dy spins. The observation of EM₁ at $\sim 30 \text{ cm}^{-1}$ may be related to irreversibility of the above sequence of phases in Fe and Dy subsystems upon sweeping of the magnetic field. Also we note, that an irreversible state of Fe spins was recently observed in DyFeO₃ at $T < T_N^{Dy}$ upon sweeping the magnetic field along the c -axis [40].

The existence of EM₁ electromagnon with a strong frequency hysteresis upon cycling of magnetic field should result in a hysteresis in the corresponding component of the static dielectric constant $\epsilon(H)$. Figure 10(a) shows the $\epsilon_c(H)$ hysteresis loop measured at 2 K in magnetic fields $H||b$ and electric field $E||c$, the latter having a sweep frequency $f = 27 \text{ kHz}$. As the field is ramped up from 0 to 2 T, $\epsilon_c(H)$ drastically drops from 24.2 to 23.1 at $\mu_0 H_{cr}^b = 0.4 \text{ T}$ when the Fe-subsystem reorients from Γ_1 to Γ_4 spin configuration. As the field is ramped down, the quasi-static ϵ partially restores at $\mu_0 H_{cr}^b = 0.4 \text{ T}$ and then, as field is further removed from 0.4 T to 0, it gradually restores to initial value of 24.1. Thus, both the EM₁ electromagnon and static ϵ demonstrate hysteresis upon cycling of magnetic field at $T < T_N^{Dy}$. We note here, that the value of critical magnetic fields H_{cr}^b at which the spin flop transition of Fe subsystem takes place is different in the IR transmittance ($\mu_0 H_{cr}^b \approx 1.3 \text{ T}$) and dielectric ($\mu_0 H_{cr}^b \approx 0.4 \text{ T}$) measurements. As it was shown in [37] the value of H_{cr}^b is sensitive to the angle β between the direction of magnetic

field and the b -axis of the crystal. Thus the observed difference in H_{cr}^b might be related to slightly different angles β in optical and dielectric measurements.

Figure 11 shows magnetic field dependence ($H||a$) of transmission spectra measured in the $e_c h_b$ configuration at $T=1.5$ K with cycling magnetic field up (a-b) and down (c-d). With increasing the field starting from $H_a=0$ the EM_1 and EM_2 electromagnons at ~ 18 cm^{-1} and ~ 48 cm^{-1} are observed up to $\mu_0 H_{cr}^a \approx 1$ T and vanish at $H > H_{cr}^a$. With decreasing the magnetic field at $H < H_{cr}^a$ the $EM_{1,2}$ appear again, but in slightly different positions: EM_1 appears at ~ 20 cm^{-1} and EM_2 - at ~ 57 cm^{-1} . We note here, that a weak shift of EM_1 and EM_2 lines was also observed in the temperature dependence of transmission spectra in the $e_c h_b$ configuration in zero magnetic field (see Fig.4): with the temperature increase from 2 K to 4 K, the EM_1 line changes its position from ~ 20 cm^{-1} to ~ 22 cm^{-1} , and EM_2 line shifts from 48 cm^{-1} to 55 cm^{-1} .

IV. DISCUSSION AND CONCLUSIONS

4.1 Quasi-FM mode hardening below T_N^{Dy}

Figure 1 shows that the frequency of the quasi-FM mode increases from 14 cm^{-1} to 19 cm^{-1} below $T_N^{Dy}=4.2$ K when the ordering of Dy spins in the ab plane occurs. The observed magnon hardening indicates a strong Dy–Fe interaction. Below T_N^{Dy} , only the lowest $|\pm 15/2\rangle$ Dy doublet is populated and thus it governs the magnetic properties of Dy subsystem at these temperatures. For our estimations we will consider Dy subsystem in a two sublattice approximation with Dy moments ordered in a collinear antiferromagnetic structure in the a - b

plane. In this case, the magnetization M_{Dy} of one of the two Dy sublattices below $T_N^{Dy}=4.2$ K can be described in the Weiss mean-field theory approach as follows:

$$M_{Dy}(H_{eff}) = N\mu_{Dy} \tanh\left(\frac{\mu_{Dy}\lambda M_{Dy}}{k_B T}\right) \quad (1)$$

Here N is a number of Dy^{3+} ions in one of the sublattices per unit volume; μ_{Dy} is a magnetic moment of a split Dy ground state doublet sublevel $\mu_{Dy} \gg 9.2\mu_B$ [3, 33]; $\tanh(x)$ is a Brillouin function $B_S(x)$ for $S=1/2$ (since only the lowest Dy doublet level is relevant); λ is a mean-field constant. Introducing reduced magnetization $m = M_{Dy}/N\mu_{Dy}$ and reduced temperature $t = Tk_B/N\mu_{Dy}^2 \lambda$ Eq.(1) can be rewritten as:

$$\begin{aligned} m &= \tanh(x) \\ m &= xt \end{aligned} \quad (2)$$

Solving graphically Eqs. (2) we obtain reduced magnetization at a given reduced temperature, where $m=1$ corresponds to the saturated magnetization $M_{Dy} = N\mu_{Dy}$ and $t=1$ corresponds to the Neel temperature $T_N^{Dy} = N\mu_{Dy}^2 \lambda/k_B$. The obtained temperature dependence of M_{Dy} is shown in inset of Fig. 1 in normalized units with black solid curve. The quasi-FM mode frequency below T_N^{Dy} can be described as follows:

$$\omega_{FM}(T) = 14 \text{ cm}^{-1} + kM_{Dy}(T) \quad (3)$$

where k is a matching coefficient. Using Eq.(3) we demonstrate that the calculated frequency $\omega_{FM}(T)$ nicely correlates with the experimental data below T_N^{Dy} (see inset of Fig.1).

4.2 Effective g-factor of the quasi-FM mode at $T < T_N^{Dy}$

Figure 6 shows that at $T=1.5$ K and $H > H_{cr}^c$, when Fe spins are in $\Gamma_4(G_x F_z)$ phase, the frequency of the quasi-FM mode linearly depends on the external magnetic field along the c -axis with effective g-factor $g_{eff} \approx 2.1$. The frequency of the quasi-FM mode can be obtained from the equations of motion of magnetic order parameters G and F:

$$\begin{aligned} \frac{d\vec{F}}{dt} &= -\gamma[\vec{F} \times \vec{H}_F] - \gamma[\vec{G} \times \vec{H}_G] \\ \frac{d\vec{G}}{dt} &= -\gamma[\vec{F} \times \vec{H}_G] - \gamma[\vec{G} \times \vec{H}_F] \end{aligned} \quad (4)$$

where $\vec{G} = (\vec{M}_1 - \vec{M}_2)/2$, $\vec{F} = (\vec{M}_1 + \vec{M}_2)/2$ are antiferro- and ferromagnetism vectors, $\vec{M}_{1,2}$ are magnetic moments of Fe sublattices, $\vec{H}_F = -\partial\Phi/\partial\vec{F}$, $\vec{H}_G = -\partial\Phi/\partial\vec{G}$, $\gamma \gg 2\mu_B/\hbar$ is the gyromagnetic ratio for Fe spins and Φ is non-equilibrium thermodynamic potential of DyFeO₃. At low temperatures when only the lowest Dy doublet is populated and Dy subsystem is paramagnetic Φ is given by the expression [36]:

$$\Phi = 1/2 A \vec{F}^2 + 1/2 \tilde{b}_2 G_y^2 + 1/2 \tilde{b}_3 G_z^2 + d_1 G_x F_z + d_3 G_z F_x - (1 + \eta_z) F_z H_z - \tau_1 G_x H_z + \text{forth order terms} \quad (5)$$

where A and $d_1 \approx -d_3 = -d$ are isotropic and antisymmetric Dzyaloshinskii-Morija constants; \tilde{b}_2 and \tilde{b}_3 are anisotropy constants renormalized by Dy-Fe interaction; $\eta_z = \chi_c \lambda_F$ and $\tau_1 \approx \chi_c \lambda_G \cos \varphi_0$, where χ_c is a Van-Vleck susceptibility of Dy ions along the c -axis, λ_F and λ_G are constants of isotropic and anisotropic Dy-Fe exchange interaction. Linearizing and solving Eqs.(4) using thermodynamic potential Φ from Eq. (5) the following expression for $\omega_{FM}(H||c)$ can be

obtained for $\Gamma_4(G_x F_z)$ phase of Fe spins: $\omega_{FM} = \sqrt{\omega_0^2 + \gamma^2 H (H + H_D^{eff})}$, where ω_0 is the magnon's frequency in zero field, $\gamma \gg \frac{2\mu_B}{\hbar}$ is the gyromagnetic ratio for Fe spins and H_D^{eff} is the effective Dzyaloshinskii field. In external magnetic fields which are small compared to H_D^{eff} the frequency ω_{FM} can be written as follows:

$$\omega_{FM} \gg \omega_0 + \frac{\gamma^2 H_D^{eff}}{2\omega_0} H \quad (6)$$

We note, that Eq. (6) was derived using thermodynamic potential (5) where Dy subsystem was considered paramagnetic. For more accurate results at $T < T_N^{Dy}$, weak interaction between Dy magnetic moments should be taken into account in the expression for thermodynamic potential Φ . At the same time as a first approximation we will use Eq. (6) to estimate Dzyaloshinskii field H_D^{eff} at $T < T_N^{Dy}$. At $T=1.5$ K ω_{FM} linearly depends on the external magnetic field along the c -axis $\omega_{FM} = \omega_{FM}^{extrap} + g_{eff} \mu_B \mu_0 H$ where $g_{eff} \approx 2.1$ and $\omega_0 = \omega_{FM}^{extrap} \approx 15.2 \text{ cm}^{-1}$ (see Fig.6(b)). Comparing this to Eq. (6) we get $\mu_0 H_D^{eff} \gg 34 \text{ T}$. Earlier room temperature (RT) studies of quasi-FM mode behavior in the magnetic field $H||c$ showed that $\mu_0 H_D^{eff}$ in DyFeO₃ is $\sim 16.5 \text{ T}$ [³¹] which is smaller by a factor of ~ 2 compared to the value we obtained for $T=1.5$ K. Taking into account that Dzyaloshinskii field H_D practically does not depend on temperature in YFeO₃ [⁴¹, ⁴²] where Y is a non-magnetic ion, the increase of H_D^{eff} at low temperatures in DyFeO₃ can be attributed to the increase of Dy–Fe interaction.

4.3 Contribution of the electromagnon EM_1 to the static ϵ upon cycling of magnetic field

$$H \parallel b \text{ at } T < T_N^{Dy}$$

To evaluate the contribution of the electromagnon excitation EM_1 to the changes in $\epsilon_c(H)$ shown in Fig. 10(a) the transmission spectra from Fig. 9 were modeled and fitted. The obtained magnetic field dependent parameters of EM_1 excitation such as oscillator strength S_{EM} , eigen frequency ω_{EM} and damping constant γ_{EM} are shown in Table II. The modeling of transmission spectra measured during ramping the field up was more complicated and less reliable as the form of EM_1 spectral line wasn't nicely fitted with one oscillator and required introduction of two closely positioned and overlapping Lorentz oscillators. For this reason in Table II we indicate only the combined oscillator strength of two Lorentz oscillators used for fit of EM_1 during ramping the field up and do not indicate eigen frequency and damping constant of EM_1 . The contribution to electric susceptibility spectrum due to the EM_1 excitation can be described using a Lorentz oscillator:

$$\chi_{EM}(\omega) = \frac{S_{EM} \omega_{EM}^2}{\omega_{EM}^2 - \omega^2 + i\gamma_{EM} \omega}. \quad (7)$$

At $\omega=0$ Eq.(7) gives EM_1 contribution to static permittivity ϵ_c : $\Delta\epsilon_{EM} = \chi_{EM}(0) = S_{EM}$ which is equal to the oscillator strength of the EM_1 excitation. Magnetic field dependence of S_{EM} from Table II is plotted in Fig. 10(a) above the high field value of $\epsilon_c \approx 23.1$ (black curve with open circles for ramping field up and red curve with open triangles for ramping field down). At low magnetic fields ($H < H_{cr}^b$) $S_{EM} \sim 0.5$ and accounts for $\sim 45\%$ of the total change of quasi-static ϵ_c during the cycling of magnetic field ($\Delta\epsilon_{\max}(1.5 K) = 24.2 - 23.1 = 1.1$). Figure 10(b) shows the

$\epsilon_c(H)$ hysteresis loop measured at $T=10$ K that is above T_N^{Dy} . At this temperature $\epsilon_c(H)$ doesn't manifest any hysteresis. At the same time ϵ_c still experiences change $\Delta\epsilon_{\max}(10\text{ K}) \approx 0.6$ during the spin-reorientation transition of Fe subsystem at $\mu_0 H_{cr}^b = 0.6 T$, which is no longer related to the contribution from the electromagnon EM_1 . The difference between total change of quasi-static ϵ_c observed during the cycling of magnetic field at $T=1.5$ K and 10 K is $\Delta\epsilon_{\max}(1.5\text{ K}) - \Delta\epsilon_{\max}(10\text{ K}) = 0.5$ which is close to the oscillator strength of EM_1 in low magnetic fields ($S_{EM} \sim 0.5$) indicating that this difference can be mainly due to contribution from the electromagnon EM_1 .

Conclusions.

In conclusion, we have studied magnetic excitations in $DyFeO_3$ single crystal in the far-IR spectral region in external magnetic fields along all three main crystallographic directions and low temperatures down to 1.5 K, *i.e.*, below T_N^{Dy} . The frequencies of both quasi-FM and quasi-AFM magnon modes demonstrate hardening upon magnetic ordering of Dy spins at $T_N^{Dy} = 4.2$ K that can be attributed to appearance of an additional effective magnetic field at Fe sites due to Dy-Fe interaction. The quasi-FM mode's g -factor along the c -axis at $T < T_N^{Dy}$ and low external magnetic fields is zero; at high enough magnetic fields when Fe subsystem is at Γ_4 spin configuration $g_{eff} = 2.1$ which is nearly twice as big as reported earlier for $T=300$ K. The increase of g_{eff} can be attributed to the renormalization of the effective Dzyaloshinskii field H_D^{eff} due to the increase of Dy-Fe interaction at low temperatures. Two electric dipole-active

magnetic excitations EM_1 and EM_2 , or electromagnons, have been found at $\sim 20\text{cm}^{-1}$ and 60cm^{-1} in the magnetoelectric phase of DyFeO_3 below T_N^{Dy} . The electromagnons vanish with the application of strong enough magnetic field along the a or b axis which changes the magnetic structures of Fe^{3+} and Dy^{3+} moments into the ones compatible with spatial inversion symmetry. We show that the electromagnon at $\sim 20\text{cm}^{-1}$ provides a significant contribution to the static electric permittivity ϵ . The energies of the electromagnons as well as static electric permittivity manifest a strong hysteresis upon cycling of external magnetic field at $T < T_N^{Dy}$.

Acknowledgments

The authors are thankful to Roman Basistyy for help with modeling of experimental data and to Sergey Artyukhin for interest and useful discussions. Work at New Jersey Institute of Technology and Rutgers University was supported by the US Department of Energy under Contract No. DE-FG02-07ER46382. Use of the National Synchrotron Light Source, Brookhaven National Laboratory, was supported by the US Department of Energy under Contract No. DE-AC02-98CH10886.

Table I. Selection rules for quasi-FM and quasi-AFM modes of AFMR in DyFeO₃ [^{31,32}]

Fe phase	quasi-FM		quasi-AFM	
	Oscillation quantities	Activity	Oscillation quantities	Activity
$\Gamma_1(G_y)$	$G_z F_x$	$h a$	$G_x F_z$	$h c$
$\Gamma_2(G_z F_x)$	$F_y F_z G_x$	$h b, h c$	$G_y F_x G_z$	$h a$
$\Gamma_4(G_x F_z)$	$G_z F_x F_y$	$h a, h b$	$G_y G_x F_z$	$h c$

Table II. Parameters of the EM₁ electromagnon [see Eq.(7)] obtained from modeling of transmission spectra of DyFeO₃ measured in $e_c h_a$ configuration at $T=1.5$ K as the magnetic field was ramped up from 0 to 2T and then down from 2 T to 0.

$\mu_0 H, T$	S_{EM1}^{up}	S_{EM1}^{down}	$\omega_{EM1}^{down}, \text{cm}^{-1}$	$\gamma_{EM1}^{down}, \text{cm}^{-1}$
2 – 1.4	0	0	-	-
1.2	0.19	0	-	-
1.0	0.36	0.43	29.8	33
0.8	0.36	0.34	29.8	30
0.6	0.39	0.44	29.4	14
0.4	0.49	0.55	30.2	15
0.2	0.52	0.57	28.5	13.4
0	0.52	0.9	17.5	9.3

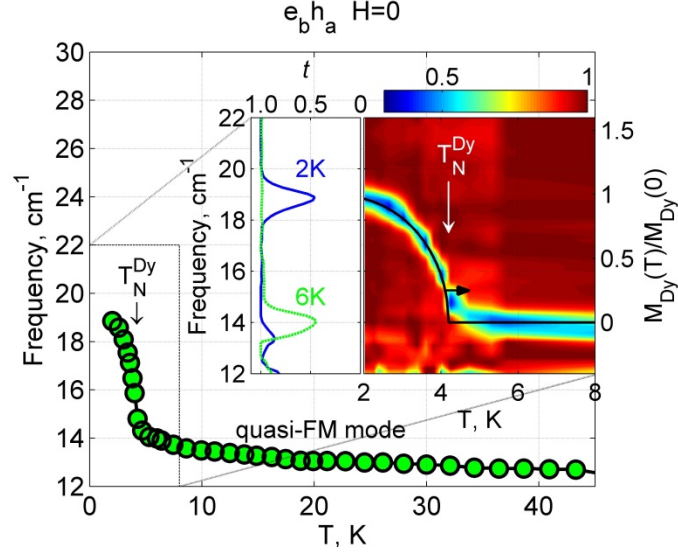


FIG 1. (Color online) Temperature dependence of the quasi-FM mode frequency (green circles) measured in DyFeO_3 single crystals in the $e_b h_a$ configuration. The right part of inset shows a normalized transmittance map vs temperature and light frequency for the temperature range around $T_N^{\text{Dy}} = 4.2$ K (left scale is for frequency). Black curve shows temperature dependence of relative changes of Dy magnetization $M_{\text{Dy}}(T)$ (right scale) calculated using Eq.(3). The left part of inset shows two spectra for normalized transmittance t measured near the region of magnon absorption at 2 K ($T < T_N^{\text{Dy}}$) and 6 K ($T > T_N^{\text{Dy}}$).

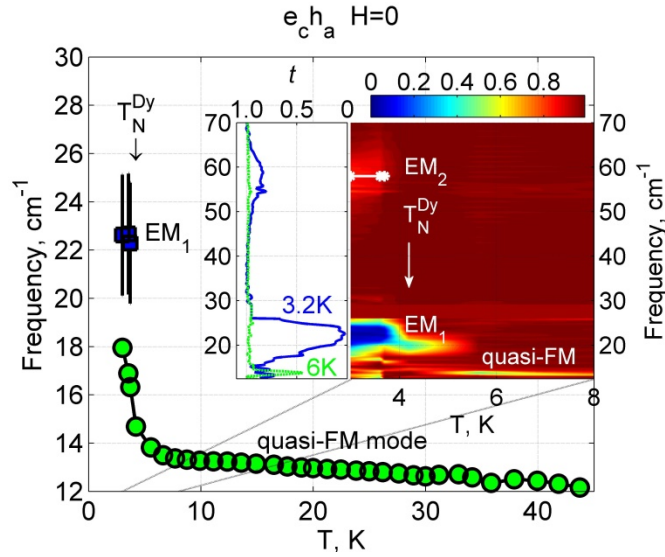


FIG 2. (Color online) Temperature dependence of the quasi-FM mode measured in the $e_c h_a$ configuration in the temperature range between 3 K and 45 K. Position of two electromagnons EM_1 and EM_2 is shown with blue squares in the temperature range below $T_N^{Dy} = 4.2$ K. The right part of inset shows a normalized transmittance map measured in the temperature range around $T_N^{Dy} = 4.2$ K. An artefact of the measurement between 27 cm^{-1} and 29 cm^{-1} , which is due to the minimum of the beamsplitter transmittance, is smeared out in the color map. The left part of inset shows two spectra for normalized transmittance t measured at 3.2 K ($T < T_N^{Dy}$) and 6 K ($T > T_N^{Dy}$).

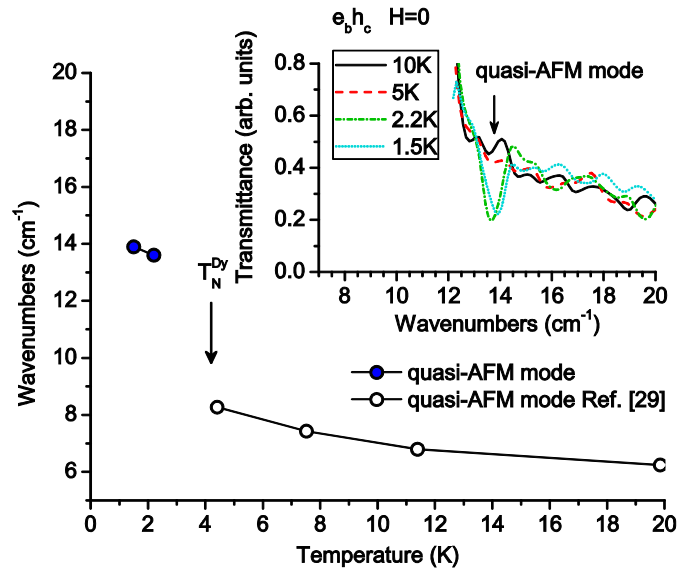


FIG 3. (Color online) Temperature dependence of the quasi-AFM mode frequency. Open circles are experimental data for the quasi-AFM mode from Ref. [29], blue circles are experimental data from this work. Inset shows four spectra of transmittance measured at $T= 1.5, 2.2, 5$ and 10 K in the $e_b h_c$ configuration.

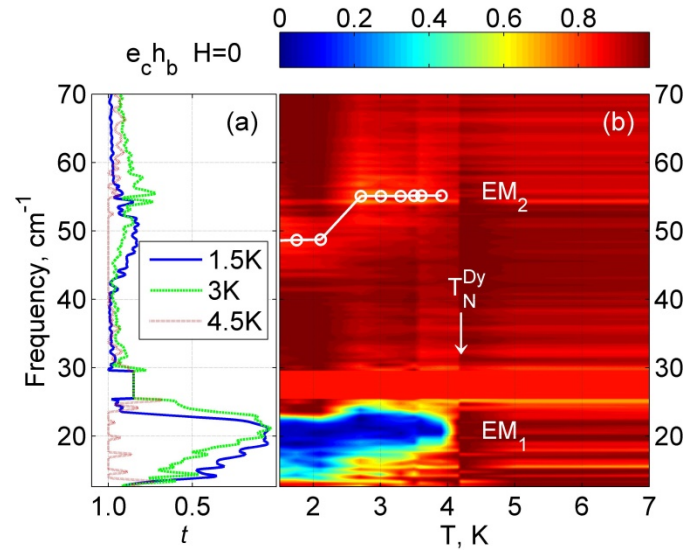


FIG 4. (Color online) Temperature dependence of normalized transmittance t measured in the $e_c h_b$ configuration in zero magnetic field ($H=0$) near the region of EM_1 and EM_2 electromagnon absorptions. (a) Three spectra for normalized transmittance t measured at $T=1.5, 3$ and 4.5 K. (b) A normalized transmittance map vs temperature and light frequency. An artefact of the measurement between 27 cm^{-1} and 29 cm^{-1} , which is due to the minimum of the beamsplitter transmittance, is smeared out in the color map.

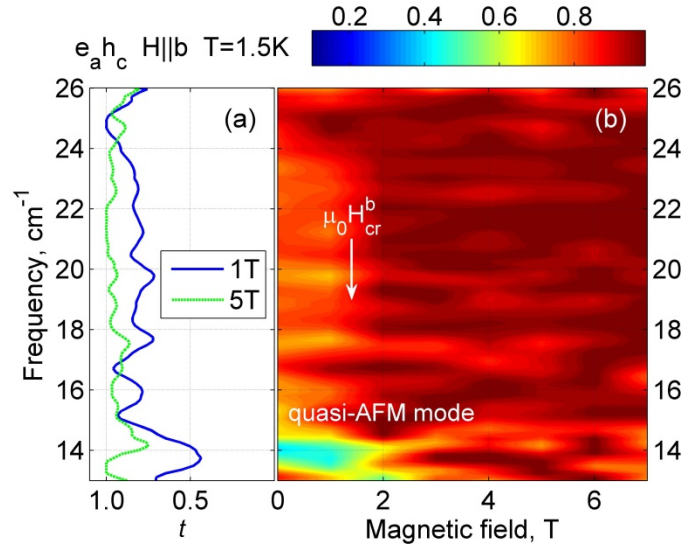


FIG 5. (Color online) Magnetic field ($H \parallel b$) dependence of normalized transmittance t measured in the $e_a h_c$ configuration at $T=1.5\text{K}$. (a) Two spectra for normalized transmittance t measured at $\mu_0 H = 1\text{ T}$ ($H < H_{cr}^b$) and 5 T ($H > H_{cr}^b$). (b) A normalized transmittance map vs magnetic field and light frequency. The quasi-AFM mode is field independent below $\mu_0 H_{cr}^b = 1.3\text{T}$.

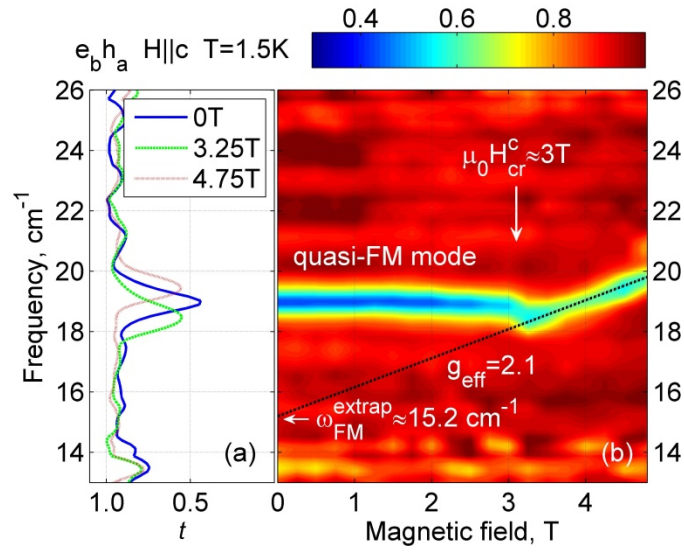


FIG 6. (Color online) Magnetic field ($H||c$) dependence of normalized transmittance t measured in the $e_b h_a$ configuration at $T=1.5$ K. (a) Three spectra for normalized transmittance t measured at $\mu_0 H = 0$ T ($H < H_{cr}^c$), 3.25 T and 4.75 T ($H > H_{cr}^c$). (b) A normalized transmittance map vs magnetic field and light frequency. Dashed straight line shows linear dependence of the quasi-FM mode on the field for $H > H_{cr}^c$ with effective g -factor of 2.1.

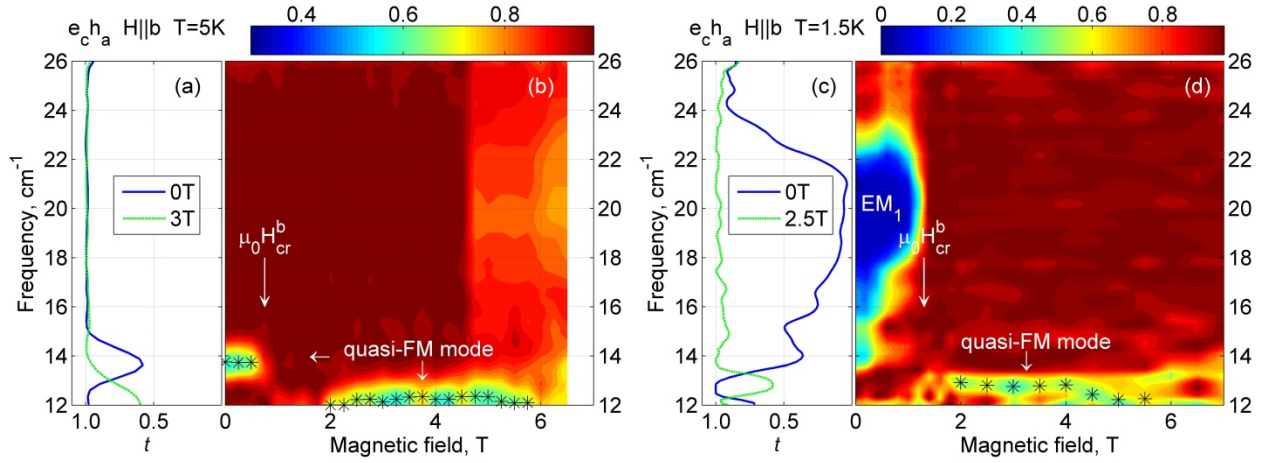


FIG 7. (Color online) Magnetic field ($H||b$) dependence of normalized transmittance t measured in the $e_c h_a$ configuration at $T=5$ K (a-b) and 1.5 K (c-d). (a) Two spectra for normalized transmittance t measured at $\mu_0 H = 0$ T ($H < H_{cr}^b$) and 3 T ($H > H_{cr}^b$). (b) A normalized transmittance map vs magnetic field ($H||b$) and light frequency measured at $T=5$ K. (c) Two spectra for normalized transmittance t measured at $\mu_0 H = 0$ T ($H < H_{cr}^b$) and 2.5 T ($H > H_{cr}^b$). (d) A normalized transmittance map vs magnetic field ($H||b$) and light frequency measured at $T=1.5$ K. Critical magnetic fields $\mu_0 H_{cr}^b$ of 0.6 T at $T=5$ K and 1.3 T at $T=1.5$ K are shown in (b) and (d) with vertical arrows. Stars in (b) and (d) show position of the quasi-FM modes.

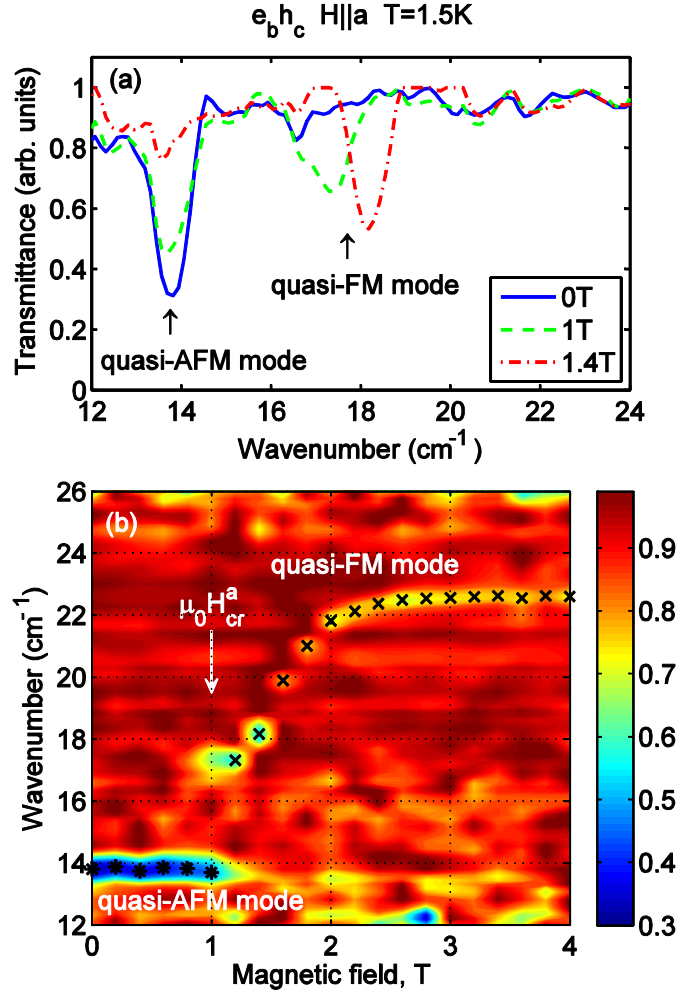


FIG 8. (Color online) Magnetic field ($H \parallel a$) dependence of normalized transmittance t measured in the $e_b h_c$ configuration at $T=1.5$ K. (a) Three spectra for normalized transmittance t measured in the interval of magnetic fields around SR transition at about $\mu_0 H_{cr}^a = 1$ T. Two AFMR modes are observed simultaneously at $H = H_{cr}^a$. (b) A normalized transmittance map vs magnetic field ($H \parallel a$) and light frequency. The positions of quasi-FM and quasi-AFM modes are marked with crosses and stars correspondingly.

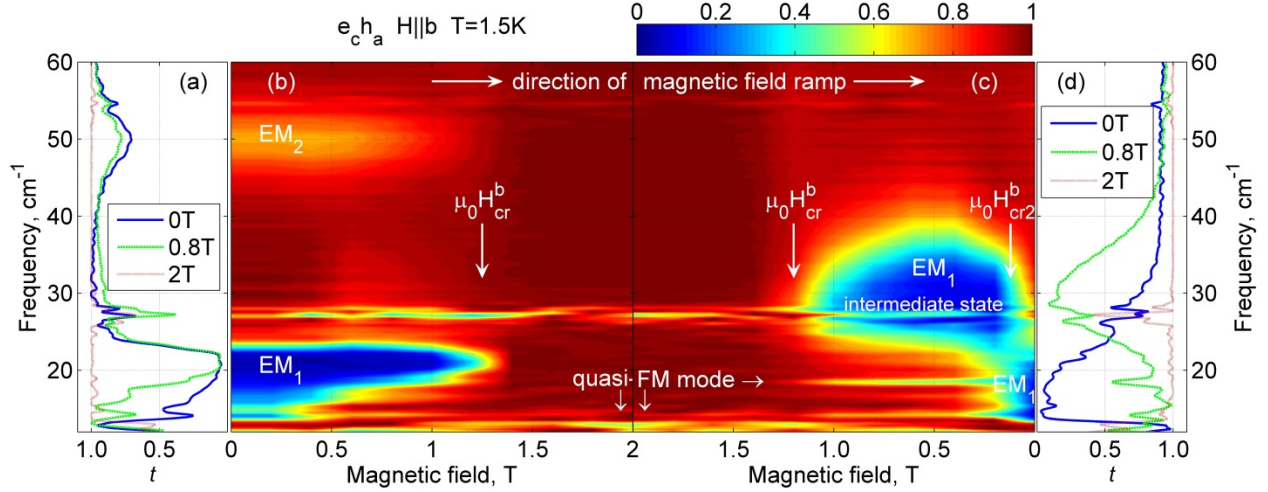


FIG 9. (Color online) Magnetic field ($H \parallel b$) dependence of normalized transmittance t measured in the $e_c h_a$ configuration at $T=1.5$ K during ramping field up (a-b) and down (c-d). (a) Three spectra for normalized transmittance t measured during ramping field up for $\mu_0 H = 0$ T, 0.8 T ($H < H_{cr}^b$) and 2 T ($H > H_{cr}^b$). (b) A normalized transmittance map vs magnetic field and light frequency measured during ramping field up. (c) A normalized transmittance map measured during ramping field down. (d) Three spectra for normalized transmittance t measured at $\mu_0 H = 0$ T ($H < H_{cr2}^b$), 0.8 T ($H_{cr2}^b < H < H_{cr}^b$) and 2 T ($H > H_{cr}^b$) during ramping field down. A quasi-FM mode is marked with white arrow. Critical magnetic fields $\mu_0 H_{cr}^b \approx 1.3$ T in (b) and (c) and $\mu_0 H_{cr2}^b \approx 0.2$ T in (c) are shown with vertical arrows. An artefact of the measurement between 27 cm^{-1} and 29 cm^{-1} is due to the minimum of the beamsplitter transmittance.

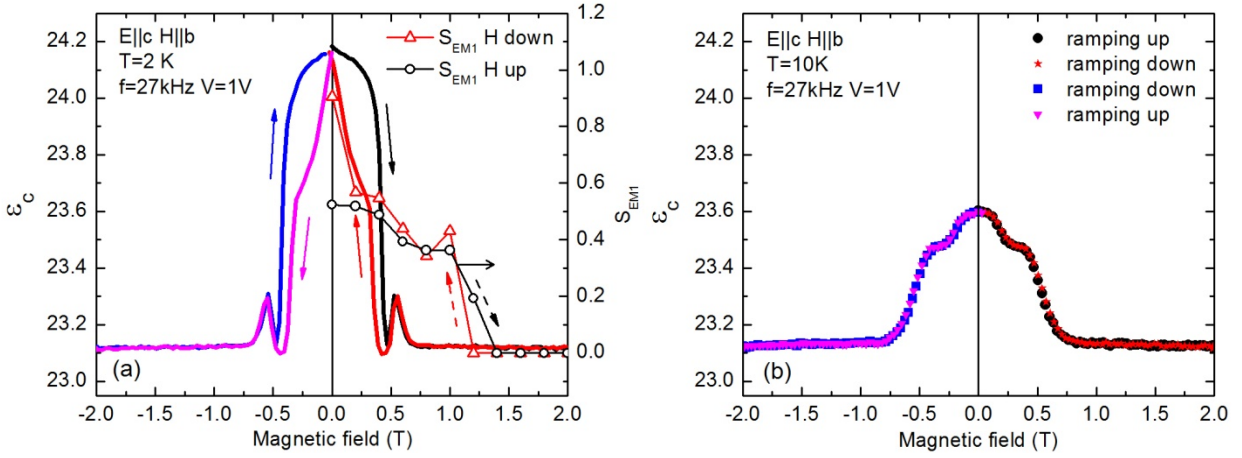


FIG 10. (Color online) Magnetic field ($H \parallel b$) dependence of electric permittivity ϵ_c of DyFeO₃ single crystal measured at $T = 2$ K (a) and 10 K (b), *i.e.*, below and above $T_N^{Dy} = 4.2$ K. Red curve with open triangles and black curve with open circles in (a) show contribution of the electromagnon EM_1 to the static ϵ . No hysteresis in $\epsilon(H)$ was observed at $T = 10$ K.

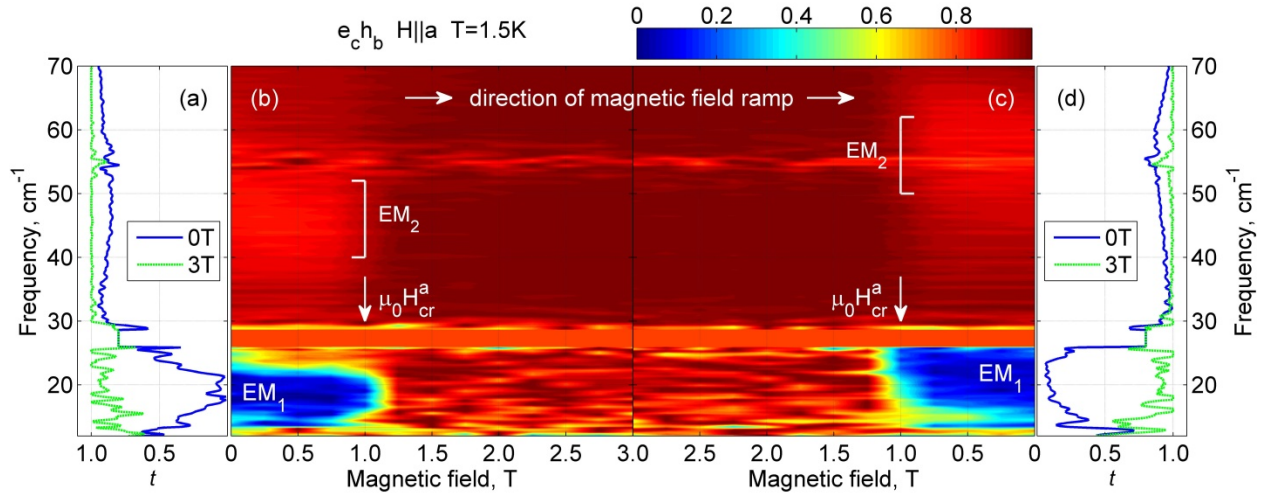


FIG 11. (Color online) Magnetic field ($H||a$) dependence of normalized transmittance t measured in the $e_c h_b$ configuration at $T=1.5$ K during ramping field up (a-b) and down (c-d). (a) Two spectra for normalized transmittance t measured at $\mu_0 H = 0$ T ($H < H_{cr}^a$) and 3 T ($H > H_{cr}^a$) during ramping field up. (b) A normalized transmittance map vs magnetic field and light frequency measured during ramping field up. (c) A normalized transmittance map measured during ramping field down. (d) Two spectra for normalized transmittance t measured at $\mu_0 H = 0$ T ($H < H_{cr}^a$) and 3 T ($H > H_{cr}^a$) during ramping field down. An artefact of the measurement between 27 cm⁻¹ and 29 cm⁻¹ is smeared out in the color map. Critical magnetic field $\mu_0 H_{cr}^a \approx 1$ T in (b) and (c) is shown with vertical arrows.

REFERENCES

- ¹ M. Marezio, J. P. Remeika and P. D. Dernier, *The Crystal Chemistry of Rare Earth Orthoferrites*, Acta Cryst. B **26**, 2008 (1970).
- ² R. L. White, *Review of Recent Work on the Magnetic and Spectroscopic Properties of the Rare-Earth Orthoferrites*, J. Appl. Phys. **40**, 1061 (1969).
- ³ G. Gorodetsky, B. Sharon, and S. Shtrikman, *Magnetic Properties of an Antiferromagnetic Orthoferrite*, J. Appl. Phys. **39**, 1371 (1968).
- ⁴ K. P. Belov, A. K. Zvezdin, A. M. Kadomtseva, and I. B. Krynetskii, *New orientational transitions induced in orthoferrites by an external field*, Sov. Phys. JETP **40**, 980 (1975).
- ⁵ A. Berton and B. Sharon, *Specific Heat of DyFeO₃ from 1.2°–80°K*, J. Appl. Phys. **39**, 1367 (1968).
- ⁶ C. E. Johnson, L. A. Prelorendjo and M. F. Thomas, *Field induced spin reorientation in orthoferrites DyFeO₃, HoFeO₃ and ErFeO₃* // J. Magn. Magn. Mater. **15-18**, 557-558 (1980).
- ⁷ Tsuyoshi Yamaguchi, Kuniro Tsushima, *Magnetic Symmetry of Rare-Earth Orthochromites and Orthoferrites*, Phys. Rev. B **8**, 5187 (1973).
- ⁸ Y. Tokunaga, S. Iguchi, T. Arima, and Y. Tokura, *Magnetic-Field-Induced Ferroelectric State in DyFeO₃*, Phys. Rev Lett. **101**, 097205 (2008).
- ⁹ N. Kida, Y. Tokura, *Terahertz magnetoelectric response via electromagnons in magnetic oxides*, J. Magn. Magn. Mat. **324**, 3512 (2012).

-
- ¹⁰ A. P. Pyatakov and A. K. Zvezdin, *Magnetoelectric and multiferroic media*, *Physics-Uspekhi* **55**, 557 (2012).
- ¹¹ V. N. Krivoruchko, *Electrically active magnetic excitations in antiferromagnets (Review Article)*, *Low Temp. Phys.* **38**, 807 (2012).
- ¹² A. Pimenov, A. M. Shuvaev, A. A. Mukhin, A. Loidl, *Electromagnons in multiferroic manganites*, *J. Phys.: Condens. Matter* **20**, 434209 (2008).
- ¹³ D. Senff, N. Aliouane, D. N. Argyriou, A. Hiess, L. P. Regnault, P. Link, K. Hradil, Y. Sidis, M. Braden, *Magnetic excitations in a cycloidal magnet: the magnon spectrum of multiferroic TbMnO₃*, *J. Phys.: Condens. Matter* **20**, 434212 (2008).
- ¹⁴ N. Kida, Y. Takahashi, J. S. Lee, R. Shimano, Y. Yamasaki, Y. Kaneko, S. Miyahara, N. Furukawa, T. Arima, Y. Tokura, *Terahertz time-domain spectroscopy of electromagnons in multiferroic perovskite manganites*, *J. Opt. Soc. Am. B* **26**, A35 (2009).
- ¹⁵ A. Pimenov, A. Shuvaev, A. Loidl, F. Schrettle, A. A. Mukhin, V. D. Travkin, V. Yu. Ivanov, and A. M. Balbashov, *Magnetic and magnetoelectric excitations in TbMnO₃*, *Phys. Rev. Lett.* **102**, 107203 (2009).
- ¹⁶ A. M. Shuvaev, V. D. Travkin, V. Yu. Ivanov, A. A. Mukhin, and A. Pimenov, *Evidence of Electroactive excitation of the spin cycloid in TbMnO₃*, *Phys. Rev. Lett.* **104**, 097202 (2010).

-
- ¹⁷ S. Pailhès, X. Fabrèges, L. P. Régnault, L. Pinsard-Godart, I. Mirebeau, F. Moussa, M. Hennion, S. Petit, *Hybrid Goldstone modes in multiferroic $YMnO_3$ studied by polarized inelastic neutron scattering*, Phys. Rev. B **79**, 134409 (2009).
- ¹⁸ A. B. Sushkov, R. Valdés Aguilar, S. Park, S-W. Cheong, H. D. Drew, *Electromagnons in Multiferroic YMn_2O_5 and $TbMn_2O_5$* , Phys. Rev. Lett. **98**, 027202 (2007).
- ¹⁹ I. Kézsmárki, N. Kida, H. Murakawa, S. Bordács, Y. Onose, Y. Tokura, *Enhanced Directional Dichroism of Terahertz Light in Resonance with Magnetic Excitations of the Multiferroic $Ba_2CoGe_2O_7$ Oxide Compound*, Phys. Rev. Lett. **106**, 057403 (2011).
- ²⁰ S.P.P. Jones , S.M. Gaw , K.I. Doig , D. Prabhakaran , E.M. Hétyey Wheeler, A.T. Boothroyd and J. Lloyd-Hughes, *High-temperature electromagnons in the magnetically induced multiferroic cupric oxide driven by intersublattice exchange*, Nat. Commun. 5:3787 doi: 10.1038/ncomms4787 (2014)
- ²¹ M. Cazayous, Y. Gallais, A. Sacuto, R. de Sousa, D. Lebeugle, D. Colson, *Possible Observation of Cycloidal Electromagnons in $BiFeO_3$* , Phys. Rev. Lett. **101**, 037601 (2008).
- ²² P. Rovillain, R. de Sousa, Y. Gallais, A. Sacuto, M. A. Méasson, D. Colson, A. Forget, M. Bibes, A. Barthélémy and M. Cazayous, *Electric-field control of spin waves at room temperature in multiferroic $BiFeO_3$* , Nat. Mater. **9**, 975 (2010).
- ²³ A. M. Kuzmenko, A. Shuvaev, V. Dziom, A. Pimenova, M. Schiebl, A. A. Mukhin, V. Yu. Ivanov, L. N. Bezmaternykh, and A. Pimenov, *Giant gigahertz optical activity in multiferroic ferroborate*, Phys. Rev. B **89**, 174407 (2014).

-
- ²⁴ N. Kida, D. Okuyama, S. Ishiwata, Y. Taguchi, R. Shimano, K. Iwasa, T. Arima, Y. Tokura, *Electric-dipole-active magnetic resonance in the conical-spin magnet $Ba_2Mg_2Fe_{12}O_{22}$* , Phys. Rev. B **80**, 220406(R) (2009).
- ²⁵ N. Kida, S. Kumakura, S. Ishiwata, Y. Taguchi, Y. Tokura, *Gigantic terahertz magnetochromism via electromagnons in the hexaferrite magnet $Ba_2Mg_2Fe_{12}O_{22}$* , Phys. Rev. B **83**, 064422 (2011).
- ²⁶ S. Seki, N. Kida, S. Kumakura, R. Shimano, Y. Tokura, *Electromagnons in the Spin Collinear State of a Triangular Lattice Antiferromagnet*, Phys. Rev. Lett. **105**, 097207 (2010).
- ²⁷ R. M. White, R. J. Nemanich, and Conyers Herring, *Light scattering from magnetic excitations in orthoferrites*, Phys. Rev. B **25**, 1822 (1982).
- ²⁸ S. Venugopalan, Mitra Dutta, A. K. Ramdas, and J. P. Remeika, *Magnetic and vibrational excitations in rare-earth orthoferrites: A Raman scattering study*, Phys. Rev. B **31**, 1490 (1985).
- ²⁹ A. M. Balbashov, A. A. Volkov, S. P. Lebedev, A. A. Mukhin, and A. S. Prokhorov, *High-frequency magnetic properties of dysprosium orthoferrite*, Sov. Phys. JETP **61**, 573 (1985).
- ³⁰ S.M.Shapiro, J.D.Axe and J.P.Remeika, *Neutron-scattering studies of spin waves in rare-earth orthoferrites*, Phys. Rev. B **10**, 2014-2021 (1974).
- ³¹ A.M. Balbashov, G.V. Kozlov, A.A. Mukhin, A.S. Prokhorov, *Submillimeter spectroscopy of antiferromagnetic dielectrics: rare-earth orthoferrites*, in High Frequency Processes in Magnetic

Materials, edited by G. Srinivasan, A. Slavin (World Scientific, Singapore, 1995), Part I, pp. 56–98.

³² V. G. Bar'yakhtar, I. M. Vitebskii, and D. A. Yablonskii, “*Symmetry and magnetic-resonance frequencies in magnetically ordered crystals*”, Sov. Phys. JETP **49**, 703 (1979).

³³ H. Schuchert, S. Hofner and R. Faulhaber, *Optical Investigation of DyFeO₃* // Z. Physik **220**, 273 (1969).

³⁴ I. Nowik and H. J. Williams, *Magnetic properties and paramagnetic relaxation of dysprosium in DyFeO₃ below the Curie point*, Phys. Lett. **20**, 154 (1966).

³⁵ K. P. Belov, A. K. Zvezdin, A. M. Kadomtseva, and I. B. Krynetskii, *New orientational transitions induced in orthoferrites by an external field*, Sov. Phys. JETP **67**, 1974 (1974).

³⁶ A. K. Zvezdin and V. M. Matveev, *Theory of the magnetic properties of dysprosium orthoferrite*, Sov. Phys. JETP **77**, 1076 (1979).

³⁷ S.L. Gnatchenko, K. Piotrowski, A. Szewczyk, R. Szymczak and H. Szymczak, *Two-step metamagnetic phase transition induced by a magnetic field parallel to the b-axis in DyFeO₃*, J. Magn. Magn. Mater. **128**, 307 (1994).

³⁸ S.L. Gnatchenko, N.F. Kharchenko, P.P. Lebedev, K. Piotrowski, H. Szymczak and R. Szymczak, *Magneto-optical studies of H-T phase diagram for DyFeO₃ (H||a)*, J. Magn. Magn. Mater. **81**, 125 (1989).

³⁹ D. A. Yablonskii and V. N. Krivoruchko, *Antiferroelectric resonance in rare-earth orthoferrites*, Fiz. Tverd. Tela 30, 3069 (1988) [Phys. Solid State **30**, 1765 (1988)].

⁴⁰ Z. Y. Zhao, X. Zhao, H. D. Zhou, F. B. Zhang, Q. J. Li, C. Fan, X. F. Sun, and X. G. Li, *Ground state and magnetic phase transitions of orthoferrite DyFeO₃*, Phys. Rev. B **89**, 224405 (2014).

⁴¹ A.M. Balbashov, A. G. Berezin, Yu. M. Gufan, G. S. Kolyadko, P. Yu. Marchukov, and E. G. Rudashevskii, *Soft mode and energy gap in spin-wave spectrum in a second-order orientational phase transition. AFMR in YFeO₃*, Sov. Phys. JETP **66**, 174 (1987).

⁴² S. Jacobs, Hugh F. Burne, and Lionel M. Levinson, *Field-Induced Spin Reorientation in YFeO₃ and YCrO₃*, J. Appl. Phys. **42**, 1631 (1971).